Quantum random walks in a coherent atomic system via electromagnetically induced transparency

Yun Li,[1] Chao Hang,[1] Lei Ma,[1] Weiping Zhang,[2] and Guoxiang Huang[2,*]

[1]*Department of Physics, East China Normal University, Shanghai 200062, China*
[2]*Department of Physics, State Key Laboratory of Precision Spectroscopy, East China Normal University, Shanghai 200062, China*
[*]*Corresponding author: gxhuang@phy.ecnu.edu.cn*

Received April 22, 2008; accepted July 24, 2008;
posted August 5, 2008 (Doc. ID 94836); published September 10, 2008

We propose a scheme to realize the quantum random walk in a coherent five-level atomic system via electromagnetically induced transparency (EIT). From optical Bloch equations describing the dynamics of the electromagnetic field and atomic population and coherence, we show that two circular-polarized components of a probe field display different dispersion properties and hence acquire different phase-shift modifications when passing through atomic cells. We demonstrate that the quantum coherence and interference owing to the EIT effect result in a low absorption of the probe field and hence provide a possibility of realizing a many-step phase-shift quantum random walk. The scheme may be used to experimentally highlight the characteristics of quantum random walk and lead to a promising application for quantum computation. © 2008 Optical Society of America

OCIS codes: 270.0270, 200.3050.

1. INTRODUCTION

It is well known that for certain computational tasks, quantum algorithms are more efficient than classical ones [1]. To date, there are several general techniques known for developing and analyzing quantum algorithms. Fourier sampling, which is typified by the seminal work of Simon [2] and Shor [3], and amplitude amplification, which originated in the seminal work of Grover [4]. Yet there is still a search for new quantum algorithms that can be practically realized. In this direction, the quantum version of some classical algorithms has also attracted much attention. Quantum random walk (QRW) is one of such example.

The concept of QRW was first proposed in 1993 by Aharonov *et al.* [5]. As a quantum analog of the classical random walk, QRWs are receiving much attention [6]. Unlike the classical case, the state of a QRW at a given time is described by probability amplitude instead of probability. Thus the behavior of QRWs displays drastic differences from that of classical random walks [7,8]. The motivation of studying quantum versions of random walks lies in both practical applications and fundamental interests. In addition, the study of QRWs provides an engine for finding not only new quantum algorithms but also an example of quantum coherent control over single atoms or photons in physical systems. The algorithms based on QRWs have also been introduced in [9,10].

Although any system designed for quantum computing can also be used to perform a QRW, most quantum computers have yet to be built on a large scale for practical application. Random walks might exhibit specifics that could ease their implementation in certain physical systems, making use of the structure of the graph underlying the walk or the character of the coin, for example. Such an implementation does not necessarily constitute a full fledged quantum computer but could still be well suited to study random walks or to solve algorithmic problems based on them. In this spirit several proposals for various physical systems have been made, including trapped ions [11], cavity QED [12,13], linear optical scheme [14,15], classical implementation [16], optical lattice [17], and Bose–Einstein condensate [18]. One- and two-dimensional QRWs in an array of optical traps for neutral atoms have been proposed [19]. Some experiments have also been reported to implement the QRW and the related algorithms [20,21].

In this paper we propose a new experimental scheme to implement a one-dimensional discrete many-step phase-shift QRW in a coherent atomic system via electromagnetically induced transparency (EIT). The essential feature of an EIT-based system is that quantum coherence and interference is induced by applying a strong coupling laser field; the absorbtion of a probe field tuned to a strong one-photon resonance can be largely suppressed and hence an initially highly opaque optical medium becomes transparent. In addition to the low optical absorption, the EIT effect can be used to slow down the propagating velocity of the probe field and study the nonlinear optics at a low light level down to single photons [22,23]. It has also been shown that ultraslow optical solitons may exist in EIT-based atomic media [24–28]. Recent studies show that the EIT technique may be applied to quantum information and computation [29–32]. In the present QRW scheme, two circular-polarized components of a

probe field are taken as 2° of freedom of a probe single-photon wave packet. They experience different dispersion properties and hence acquire different phase-shift modifications, which are used to realize a phase-shift QRW. The low absorption owing to the EIT effect makes it possible to execute enough iterations in atomic cells and hence provide the possibility to realize the many-step QRW.

This paper is organized as follows. Section 2 describes the physical model based on a coherent five-level atomic system with an EIT configuration. Section 3 presents a brief introduction of a one-dimensional QRW and gives a detailed discussion about the implementation of the QRW with the EIT-based system. Finally, Section 4 contains a discussion and summary of our main results.

2. PHYSICAL MODEL

We consider a cold lifetime-broadened five-level atomic system that interacts with a weak pulsed probe field of central frequency $\omega_p/(2\pi)$ and a strong continuous-wave coupling field of frequency $\omega_c/(2\pi)$ [see Fig. 1(a)]. The system can be realized in Zeeman-split alkali atoms, such as a Rubidium atomic gas, with an $nS-nP-nD$ level scheme. Here, n denotes the principal quantum number while S, P, and D denote the azimuthal quantum numbers characterizing the angular momentum. The atomic gas is trapped in a cell with enough low temperature to cancel Doppler broadening and atomic collisions. The probe field is tuned to the lower $nS\leftrightarrow nP$ transition and propagates along the direction of an external magnetic field $\mathbf{B}$ while the coupling field is tuned to the upper $nP\leftrightarrow nD$ transition, and its propagating direction is perpendicular to the external magnetic field. Notice that a similar system has also been proposed to study long-range interactions and entanglement of slow single-photon pulses [33]. To implement a QRW different from the classical one, we need at least four atomic cells in a row with identical length and Hadamard gates located before each cell. The possible experimental apparatus for the QRW is shown in Fig. 1(b).

The electric field vector of the system can be written as $\mathbf{E}=(\hat{\mathbf{x}}\boldsymbol{\varepsilon}_{px}+\hat{\mathbf{y}}\boldsymbol{\varepsilon}_{py})\exp[i(k_pz-\omega_pt)]+\hat{\mathbf{e}}_c\boldsymbol{\varepsilon}_c\exp[i(k_cr-\omega_ct)]+\text{c.c.}$, where $r=x$ or y, $\hat{\mathbf{x}}$, $\hat{\mathbf{y}}$, and $\hat{\mathbf{e}}_c$ are the unit vectors denoting the polarization directions of the probe and coupling laser fields with relevant envelopes represented by $\boldsymbol{\varepsilon}_{px}$, $\boldsymbol{\varepsilon}_{py}$, and $\boldsymbol{\varepsilon}_c$, respectively. Using the relations $\hat{\mathbf{x}}=(\hat{\epsilon}_+ + \hat{\epsilon}_-)/\sqrt{2}$ and $\hat{\mathbf{y}}=(\hat{\epsilon}_+ - \hat{\epsilon}_-)/(i\sqrt{2})$, where $\hat{\epsilon}_+$ and $\hat{\epsilon}_-$ are the unit vectors denoting, respectively, right-circularly (σ^+) and left-circularly (σ^-) polarizations, the probe pulse can be considered as a superposition of the σ^+ and σ^- components, i.e., $\mathbf{E}_p=(\hat{\epsilon}_+\varepsilon_{p+}+\hat{\epsilon}_-\varepsilon_{p-})\exp[i(k_pz-\omega_pt)]+\text{c.c.}$ with $\boldsymbol{\varepsilon}_{p+}=(\boldsymbol{\varepsilon}_{px}-i\boldsymbol{\varepsilon}_{py})/\sqrt{2}$ and $\boldsymbol{\varepsilon}_{p-}=(\boldsymbol{\varepsilon}_{px}+i\boldsymbol{\varepsilon}_{py})/\sqrt{2}$. The σ^- component of the probe field drives the transition $|1\rangle\rightarrow|2\rangle$, and the σ^+ component drives the transition $|1\rangle\rightarrow|3\rangle$. The linearly ($\pi$) polarized coupling field drives the transitions $|2\rangle\rightarrow|4\rangle$ and $|3\rangle\rightarrow|5\rangle$. Thus both σ^+ and σ^- components of the probe field form an EIT ladder configuration with the coupling field. In an interaction picture, the evolution equations for atomic populations σ_{ii} ($i=1-5$) are

$$\dot{\sigma}_{11}=-i[\Omega_{p1}^*\sigma_{21}+\Omega_{p2}^*\sigma_{31}-\Omega_{p1}\sigma_{12}-\Omega_{p2}\sigma_{13}]+\Gamma_{21}\sigma_{22}+\Gamma_{31}\sigma_{33}+\Gamma_{41}\sigma_{44}+\Gamma_{51}\sigma_{55}, \tag{1a}$$

$$\dot{\sigma}_{22}=-i[\Omega_{p1}\sigma_{12}+\Omega_c^*\sigma_{42}-\Omega_{p1}^*\sigma_{21}-\Omega_c\sigma_{24}]-\Gamma_2\sigma_{22}+\Gamma_{42}\sigma_{44}+\Gamma_{52}\sigma_{55}, \tag{1b}$$

$$\dot{\sigma}_{33}=-i[\Omega_{p2}\sigma_{13}+\Omega_c^*\sigma_{53}-\Omega_{p2}^*\sigma_{31}-\Omega_c\sigma_{35}]-\Gamma_3\sigma_{33}+\Gamma_{43}\sigma_{44}+\Gamma_{53}\sigma_{55}, \tag{1c}$$

$$\dot{\sigma}_{44}=-i[\Omega_c\sigma_{24}-\Omega_c^*\sigma_{42}]-\Gamma_4\sigma_{44}, \tag{1d}$$

$$\dot{\sigma}_{55}=-i[\Omega_c\sigma_{35}-\Omega_c^*\sigma_{53}]-\Gamma_5\sigma_{55}, \tag{1e}$$

and the evolution equations for atomic coherence σ_{ij} ($i\neq j$, $i,j=1-5$) read

$$\dot{\sigma}_{12}=-i[\Omega_{p1}^*(\sigma_{22}-\sigma_{11})+\Omega_{p2}^*\sigma_{32}-\Omega_c\sigma_{14}+\Delta_p\sigma_{12}]-\frac{\Gamma_{21}+\gamma_{12}}{2}\sigma_{12}, \tag{2a}$$

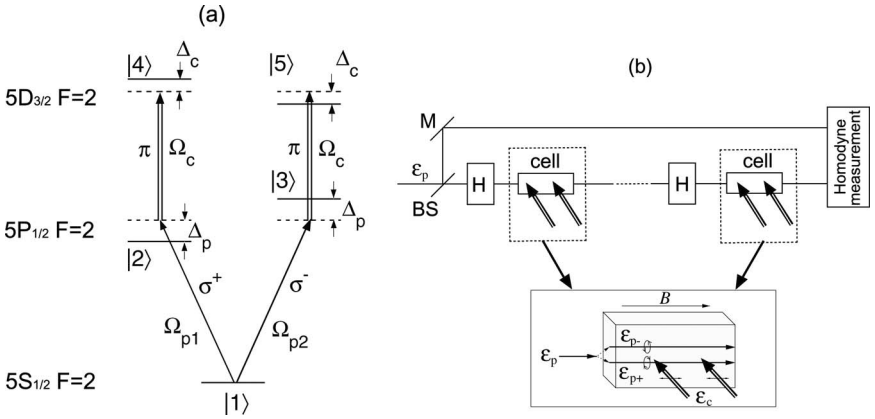

Fig. 1. (a) Energy level diagram and excitation scheme of a lifetime-broadened five-level atomic system that interacts with a weak pulsed probe field of Rabi frequency Ω_p and a strong continuous-wave coupling field of Rabi frequency Ω_c; Δ_p and Δ_c are relevant one- and two-photon detunings. The linearly polarized probe field can be considered as a superposition of the right (σ^+) and left (σ^-) circular-polarized components with the Rabi frequencies Ω_{p1} and Ω_{p2}, respectively. (b) Possible experimental apparatus. H, Hadamard gate; BS, beam splitter; M, high reflective mirror.

$$\dot{\sigma}_{13} = -i[\Omega_{p1}^{*}\sigma_{23} + \Omega_{p2}^{*}(\sigma_{33} - \sigma_{11}) - \Omega_c\sigma_{15} - \Delta_p\sigma_{13}] - \frac{\Gamma_{31} + \gamma_{13}}{2}\sigma_{13}, \tag{2b}$$

$$\dot{\sigma}_{14} = -i[\Omega_{p1}^{*}\sigma_{24} + \Omega_{p2}^{*}\sigma_{34} - \Omega_c^{*}\sigma_{12} - \Delta_c\sigma_{14}] - \frac{\Gamma_4 + \gamma_{14}}{2}\sigma_{14}, \tag{2c}$$

$$\dot{\sigma}_{15} = -i[\Omega_{p1}^{*}\sigma_{25} + \Omega_{p2}^{*}\sigma_{35} - \Omega_c^{*}\sigma_{13} + \Delta_c\sigma_{15}] - \frac{\Gamma_5 + \gamma_{15}}{2}\sigma_{15}, \tag{2d}$$

$$\dot{\sigma}_{23} = -i[\Omega_{p1}\sigma_{13} + \Omega_c^{*}\sigma_{43} - \Omega_{p2}^{*}\sigma_{21} - \Omega_c\sigma_{25} - 2\Delta_p\sigma_{23}] - \frac{\Gamma_{21} + \Gamma_{31} + \gamma_{23}}{2}\sigma_{23}, \tag{2e}$$

$$\dot{\sigma}_{24} = -i[\Omega_{p1}\sigma_{14} + \Omega_c^{*}(\sigma_{44} - \sigma_{22}) - (\Delta_c + \Delta_p)\sigma_{24}] - \frac{\Gamma_{21} + \Gamma_4 + \gamma_{24}}{2}\sigma_{24}, \tag{2f}$$

$$\dot{\sigma}_{25} = -i[\Omega_{p1}\sigma_{15} + \Omega_c^{*}(\sigma_{45} - \sigma_{23}) + (\Delta_c - \Delta_p)\sigma_{25}] - \frac{\Gamma_{21} + \Gamma_5 + \gamma_{25}}{2}\sigma_{25}, \tag{2g}$$

$$\dot{\sigma}_{34} = -i[\Omega_{p2}\sigma_{14} + \Omega_c^{*}(\sigma_{54} - \sigma_{32}) - (\Delta_c - \Delta_p)\sigma_{34}] - \frac{\Gamma_{31} + \Gamma_4 + \gamma_{34}}{2}\sigma_{34}, \tag{2h}$$

$$\dot{\sigma}_{35} = -i[\Omega_{p2}\sigma_{15} + \Omega_c^{*}(\sigma_{55} - \sigma_{33}) + (\Delta_c + \Delta_p)\sigma_{35}] - \frac{\Gamma_{31} + \Gamma_5 + \gamma_{35}}{2}\sigma_{35}, \tag{2i}$$

$$\dot{\sigma}_{45} = -i[\Omega_c\sigma_{25} - \Omega_c^{*}\sigma_{43} + 2\Delta_c\sigma_{45}] - \frac{\Gamma_4 + \Gamma_5 + \gamma_{45}}{2}\sigma_{45}, \tag{2j}$$

where $\Omega_{p1} = -(\mathbf{p}_{SP}\cdot\hat{\epsilon}_+\boldsymbol{\varepsilon}_{p+})/\hbar$, $\Omega_{p2} = -(\mathbf{p}_{SP}\cdot\hat{\epsilon}_-\boldsymbol{\varepsilon}_{p-})/\hbar$, and $\Omega_c = -(\mathbf{p}_{PD}\cdot\hat{\mathbf{e}}_c\boldsymbol{\varepsilon}_c)/\hbar$ are the Rabi frequencies with $\mathbf{p}_{SP}$ ($\mathbf{p}_{PD}$) being the electric dipole matrix element associated with the transition $nS \leftrightarrow nP$ ($nP \leftrightarrow nD$); $\Delta_p = \mu_B g_F^p B/\hbar$ ($\Delta_c = \mu_B g_F^d B/\hbar$) is the detuning of the right-circularly (left-circularly) polarization component of the probe field with μ_B being the Bohr magneton and g_F^p (g_F^d) being the Landé factor of the level nP (nD); $\Gamma_4 = \Gamma_{41} + \Gamma_{42} + \Gamma_{43}$ and $\Gamma_5 = \Gamma_{51} + \Gamma_{52} + \Gamma_{53}$ are total decay rates of the states $|4\rangle$ and $|5\rangle$, with Γ_{ij} denoting the spontaneous emission decay rate from state $|i\rangle$ to state $|j\rangle$ and γ_{ij} denoting the dephasing rate.

The electric susceptibilities $\chi_\pm$ for the σ^+ and σ^- components of the probe field are given by

$$\chi_+ = -\frac{N_a|\mathbf{p}_{SP}|^2}{\hbar\epsilon_0}\frac{\sigma_{21}}{\Omega_{p1}}, \quad \chi_- = -\frac{N_a|\mathbf{p}_{SP}|^2}{\hbar\epsilon_0}\frac{\sigma_{31}}{\Omega_{p2}}, \tag{3}$$

where N_a is the density of the atomic gas and ϵ_0 is the vacuum dielectric constant. We assume that the particles in the system are initially populated in the state $|1\rangle$. If the intensity of the probe field is much weaker than that of the coupling field, the depletion of the ground state $|1\rangle$ is not significant and hence one has $\sigma_{11} \approx 1$, $\sigma_{ii} \approx 0$ ($i = 2$ to 5), and $\sigma_{ij} \approx 0$ ($i, j = 2$ to 5, $i \neq j$). The solutions for σ_{21} and σ_{31} in the linear regime can be readily obtained using the Fourier transform technique as in [24,25]. As a result susceptibilities of the two polarization components of the probe field are given by

$$\chi_+ = -\frac{N_a|\mathbf{p}_{SP}|^2}{\hbar\epsilon_0}\frac{[|\Omega_c|^2 + \Delta_p\Delta_c + \Gamma_P\Gamma_D + i(\Delta_p\Gamma_D - \Delta_c\Gamma_P)](\Delta_c - i\Gamma_D)}{|\Omega_c|^4 + 2(\Delta_p\Delta_c + \Gamma_P\Gamma_D)|\Omega_c|^2 + (\Delta_p^2 + \Gamma_P^2)(\Delta_c^2 + \Gamma_D^2)}, \tag{4a}$$

$$\chi_- = \frac{N_a|\mathbf{p}_{SP}|^2}{\hbar\epsilon_0}\frac{[|\Omega_c|^2 + \Delta_p\Delta_c + \Gamma_P\Gamma_D - i(\Delta_p\Gamma_D - \Delta_c\Gamma_P)](\Delta_c + i\Gamma_D)}{|\Omega_c|^4 + 2(\Delta_p\Delta_c + \Gamma_P\Gamma_D)|\Omega_c|^2 + (\Delta_p^2 + \Gamma_P^2)(\Delta_c^2 + \Gamma_D^2)}, \tag{4b}$$

at $\omega = 0$ (ω denotes a frequency deviation from the center frequency of the probe field ω_p). For simplicity we have set $\Gamma_{21} \simeq \Gamma_{31} = \Gamma_P$ and $\Gamma_4 \simeq \Gamma_5 = \Gamma_D$; γ_{ij} is much less than Γ_P and Γ_D.

In Fig. 2 we have shown the dispersion spectrum Re $\chi_\pm$ [panel (a)] and absorption spectrum Im $\chi_\pm$ [panel (b)] of Ω_{p1} (solid curves) and Ω_{p2} (dashed curves), which correspond to the real part and the imaginary part of the respective susceptibilities. In plotting Fig. 2 a realistic set of system parameters (see Subsection 3.B) have been adopted. We see that the atomic medium is transparent to both polarization components of the probe field near $\omega = 0$, where normal dispersion also occurs. The physical reason for this transparency is owing to the quantum in-

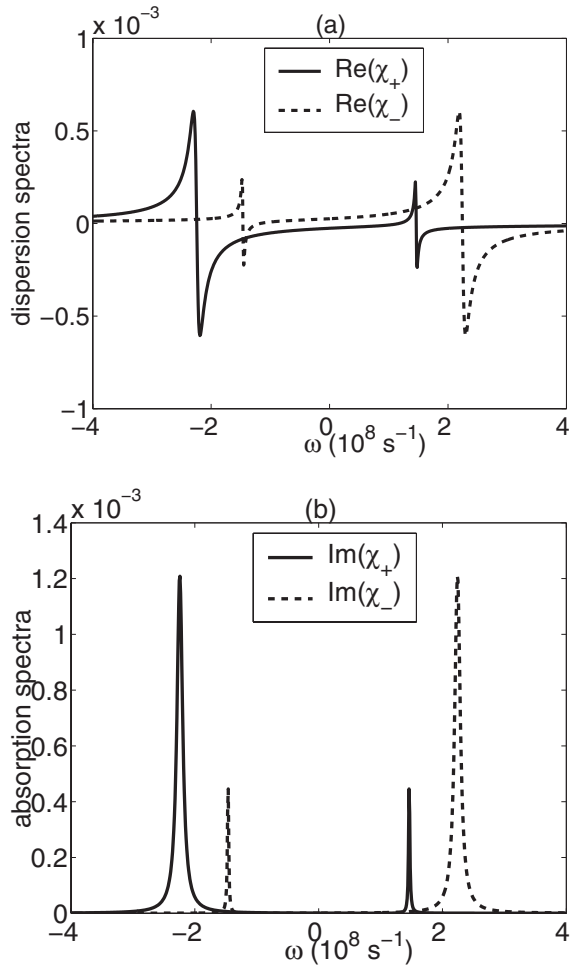

Fig. 2. (a) Dispersion (Re $\chi_{\pm}$) and absorption (Im $\chi_{\pm}$) spectra for Ω_{p1} (solid curve) and Ω_{p2} (dashed curve) with a particular set of parameters (see Subsection 3.B). (b) Absorption spectra for Ω_{p1} (solid curve) and Ω_{p2} (dashed curve) with the same parameters.

terference effect (i.e., the EIT effect) induced by the coupling field, which makes the QRW possible in the present resonant atomic system.

3. IMPLEMENTATION OF A PHASE-SHIFT QUANTUM RANDOM WALK

A. One-Dimensional Quantum Random Walk

Before the discussion of physical implementation of a QRW in the EIT-based coherent atomic system, for completeness we give a simple introduction of a QRW on a line. A discrete-time QRW can be realized by repeatedly applying a unitary evolution operator $\hat{U}$ on a Hilbert space formed by tensor product $\mathcal{H}^C \otimes \mathcal{H}^P$, where $\mathcal{H}^C$ is called a coin Hilbert space and $\mathcal{H}^P$ is called a position Hilbert space. For a line with grid-length 1, $\mathcal{H}^P$ is spanned by basis $\{|x\rangle : x \in \mathbb{Z}\}$, which indicates the site where a particle is located in. $\mathcal{H}^C$ is spanned by two basis states $|R\rangle$ and $|L\rangle$. At each time interval the particle can move one step to either the left site or the right site, each direction with 1/2 probability. The state in $\mathcal{H}^C$ determines the direction of the motion of the particle. The conditional translation $\hat{S}$ thus has the following action on the basis states:

$$\hat{S}|R,x\rangle = |R,x+1\rangle, \quad \hat{S}|L,x\rangle = |L,x-1\rangle. \tag{5}$$

In each iteration the quantum walk is implemented by the Hadamard operation,

$$\hat{H} = \frac{1}{\sqrt{2}}\begin{pmatrix} 1 & 1 \\ 1 & -1 \end{pmatrix}, \tag{6}$$

on the coin states to bring them into a superposition state with equal probability. The Hadamard operation is a necessary part of the quantum walk and works pro in many quantum algorithms. Then, the evolution operator $\hat{U}$ is given by $\hat{U} = \hat{S} \cdot (\hat{H} \otimes \hat{I})$. Let $|\psi_N\rangle = (\hat{U})^N |\psi_0\rangle$ be the state of the system after N iterations. The probability $p(x,N)$ to observe a particle in the position space after N iterations is given by

$$p(x,N) = \langle x|Tr(|\psi_N\rangle\langle\psi_N|)|x\rangle. \tag{7}$$

The probability distribution arising from repeated applications of $\hat{U}$ (i.e., quantum walk) is significantly different from the distribution from a classical walk. It is well known that for the classical random walk on a line the probability of the particle at a certain site approaches a Gaussian function centered around its initial position after a large number of iterations. However, the quantum version of such a walk displays very different behavior. If we start with the state $|\psi_0\rangle = |R,0\rangle$, by repeatedly applying the evolution operator $\hat{U}$, we will obtain a right-biased probability distribution; if we start from the state $|\psi_0\rangle = |L,0\rangle$, we will get a left-biased distribution. The variance of the quantum walk grows quadratically with the number of iterations N, i.e., $\sigma^2 \propto N^2$, which is very different from the classical result $\sigma^2 \propto N$. The physical reason for the differences between the quantum and classical walks is owing to the interference effect existing intrinsically in quantum systems.

B. Implementation of Quantum Walk in Coherent Atomic Systems

Now we present a possible scheme for the implementation of the QRW based on the coherent atomic system via EIT. In our scheme the coin Hilbert space $\mathcal{H}^C$ is spanned by the two different polarization components of the probability field, i.e., $\{|L\rangle = |\sigma^+\rangle, |R\rangle = |\sigma^-\rangle\}$. The position Hilbert space $\mathcal{H}^P$ is spanned by the phases of both polarization components and augmented by the coin Hilbert space. The state space used for the QRW is the tensor product of the "coin" and "position" spaces, i.e., $\mathcal{H}^C \otimes \mathcal{H}^P$.

As in [29–32], we assume that the input probe field is prepared as a polarized single-photon wave packet, which can be expressed as a superposition of two circular-polarized states, i.e., $|\psi\rangle = \alpha^-|\sigma^-\rangle + \alpha^+|\sigma^+\rangle$, where $|\sigma^{\pm}\rangle = \int d\omega \xi(\omega) a_{\pm}^{\dagger}(\omega)|0\rangle$ with $\xi(\omega)$ being a Gaussian distribution of incident wave packets centered at the frequency ω_p. The photon field operators undergo a transformation while propagating through the atomic medium of length L, i.e., $a_{\pm}(\omega) \to a_{\pm}(\omega)\exp\{i\omega_p n_{\pm}(\omega)L/c\}$, where $n_{\pm}(\omega)$ is the real part of the refractive index. If $n_{\pm}(\omega)$ varies slowly over the bandwidth of the wave packet, one gets $|\sigma^{\pm}\rangle \to \exp(-i\phi_{\pm})|\sigma^{\pm}\rangle$ with $\phi_{\pm} = \omega_p n_{\pm}(\omega_p)L/c \simeq \omega_p L/c + \omega_p \mathrm{Re}[\chi_{\pm}]L/(2c) \equiv \phi_0 + \Delta\phi_{\pm}$, where $\Delta\phi_{\pm}$ is the phase-shift

modification. Under a realistic set of parameters, $|\Delta\phi_+| = |\Delta\phi_-| = \Delta\phi$ can be satisfied. The transmission of the output of the two polarization components can be characterized by $T_\pm = \exp(-\alpha_\pm L)$. Owing to the EIT effect, we have $T_\pm \simeq 1$, i.e., the absorption of the probe field can be negligibly small.

In each iteration of the QRW, we first apply the Hadamard operation to the coin space, i.e., each polarization component of the single-photon wave packet is brought into a superposition of two circular states with equal probability,

$$\hat{H}|\sigma^\pm, \phi_k\rangle = \frac{1}{\sqrt{2}}[|\sigma^\pm, \phi_k\rangle \pm |\sigma^\mp, \phi_k\rangle]. \tag{8}$$

Experimentally, one can realize the above transformation by placing two $-\pi/2$ phase shifters at the input and output ports and a lossless symmetric beam splitter between them. A lossless symmetric beam splitter supplemented with two $-\pi/2$ phase shifters can be viewed as a Hadamard gate acting on a location qubit [34]. Second, both probe field circular components propagate through a single atomic cell of length L, and their phases move a step to either the left site or the right site, i.e.,

$$\hat{S}|\sigma^\pm, \phi_k\rangle = |\sigma^\pm, \phi_{k\mp 1}\rangle, \tag{9}$$

with $\phi_k = \phi_0 + k\Delta\phi$ $(k = 0, 1, 2, \ldots)$. Thus we complete one iteration of the QRW. Finally, the QRW is implemented by the repeated action on the state of the operator $\hat{H}$ and $\hat{S}$; after N iterations the final state $|\psi(N)\rangle = [\hat{S}\hat{H}]^N|\psi(0)\rangle$, which can be written as

$$|\psi(N)\rangle = \sum_{k=-N}^{N} [R_{k,N}|\sigma^+, \phi_k\rangle + L_{k,N}|\sigma^-, \phi_k\rangle], \tag{10}$$

with the probability amplitude of the right- and left-circularly polarization states with ϕ_k at the N iteration

$$R_{k,N} = \frac{1}{\sqrt{2}}(R_{k-1,N-1} + L_{k+1,N-1}), \tag{11a}$$

$$L_{k,N} = \frac{1}{\sqrt{2}}(R_{k-1,N-1} - L_{k+1,N-1}), \tag{11b}$$

where $R_{k,0} = L_{k,0} = 0$ if $k \neq 0$ and $R_{k,-1} = L_{k,-1} = 0$. Equations (11a) and (11b) are the standard QRW equations [16].

To demonstrate the possibility of the physical implementation of the QRW, we consider the cells of cold ^{85}Rb atomic gases. The experimental parameters are chosen as $B \simeq 20$ G, $\Gamma_{21} \simeq \Gamma_{31} = 5.9$ MHz $(F=2,\ 5P_{1/2})$, $\Gamma_4 \simeq \Gamma_5 = 0.8$ MHz $(F=2,\ 5D_{3/2})$, and $N_a = 7.5\times 10^9$ cm^{-3}. The detunings are given as $\Delta_p = 1.95\times 10^8$ s^{-1} and $\Delta_c = 1.17\times 10^8$ s^{-1} (the Landé factor $g_F^p = -1/9$ for the level $F=2$, $5P_{1/2}$ and $g_F^d = 1/15$ for the level $F=2$, $5D_{3/2}$, which have been used to calculate the detunings). The undesirable atom field couplings can be excluded owing to the far-off resonance. The Rabi frequency of the coupling field is $\Omega_c = 1.0\times 10^8$ s^{-1} and the probe field is $\Omega_p = 1.0\times 10^6$ s^{-1}. Thus, the probe field intensity $I_p = \frac{c}{2}\epsilon_0|\mathbf{E}_p|^2 = 6.5\times 10^{-6}$ W cm^{-2}. We remark that the intensity of a single 800 nm photon per nanosecond on an area of 1 μm is $I_{ph} = 2.5\times 10^{-2}$ W cm^{-2}. This shows that our scheme can be operated with single photons. The length of each atomic cell is taken as $L = 0.2$ cm. With the above parameters, we obtain $\chi_\pm = \mp 2.57\times 10^{-5} + i3.02\times 10^{-7}$. We see that the imaginary parts of the probe field susceptibilities for both components are much less than their relevant real parts. Thus the absorption of the system is greatly suppressed, and the coherence is well preserved. The transmission and the rotation angle for each single cell are given by $T_+ = T_- = 0.995$, $\phi_0 = 5000\pi$ rad, $\Delta\phi_+ = -0.2$ rad, and $\Delta\phi_- = 0.2$ rad. We see that large rotations with extremely small absorption for both probe field circular components are realized in each atomic cell owing to the EIT effect induced by the coupling field.

We consider the QRW that is implemented in many atomic cells arranged on a line. Each atomic cell has the parameters given above. Then, the grid-length of the position space is $\Delta\phi = 0.2$ rad. To investigate the quantum walk we take two particular initial states. The first one is $\mathbf{E}_p(z=0) = \hat{\mathbf{x}}\mathcal{E}_{px}\exp(-i\omega_p t) + \text{c.c.}$ (i.e., $\mathcal{E}_{py} = 0$), and the second one is $\mathbf{E}_p(z=0) = (\hat{\mathbf{x}} + \hat{\mathbf{y}})\mathcal{E}_p \exp(-i\omega_p t) + \text{c.c.}$ (i.e., $\mathcal{E}_{py} = \mathcal{E}_{py} = \mathcal{E}_p$). In Fig. 3 we have shown the quadrature phase distribution (QPD) after five iterations. The black (gray) histogram (QW1) (QW2) is the result for the distribution calculated from the first (second) initial state. The white histogram denotes the distribution of corresponding classical walk (CW). The abscissa in the figure is sin ϕ. From Fig. 3 we see that owing to the quantum interference effect of the system, the shape of the distribution function is right-biased when starting from the first initial state and unbiased from the second initial state. The distribution functions of the quantum walk are quite different from the classical one.

In addition, we have also simulated the outcome of homodyne measurement and thereby obtained the related QPD on the orthogonal axis to the initial coherent state. The simulated variance of the QPD as a function of the number of iterations is given in Fig. 4. From Fig. 4 we see that the variance of the quantum walk is basically iden-

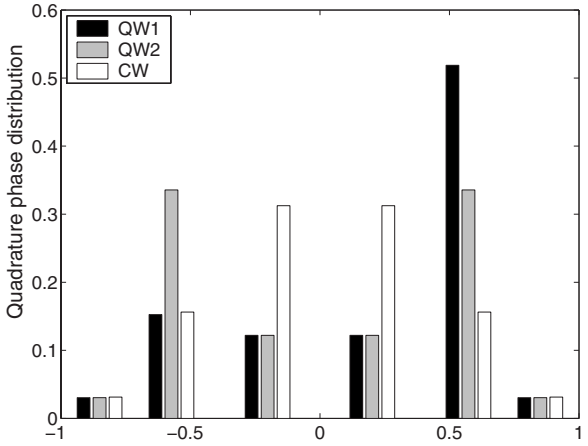

Fig. 3. QPD after five iterations, where QW1 (black histogram) denotes the distribution calculated from the initial state $\mathbf{E}_p$ $(z=0) = \hat{\mathbf{x}}\mathcal{E}_{px}\exp(-i\omega_p t) + \text{c.c.}$ (i.e., $\mathcal{E}_{py} = 0$), QW2 (gray histogram) denotes the distribution calculated from the initial state $\mathbf{E}_p$ $(z=0) = (\hat{\mathbf{x}} + \hat{\mathbf{y}})\mathcal{E}_p \exp(-i\omega_p t) + \text{c.c.}$ (i.e., $\mathcal{E}_{py} = \mathcal{E}_{py} = \mathcal{E}_p$), and CW (white histogram) denotes the distribution of a classical walk. The abscissa is sin ϕ.

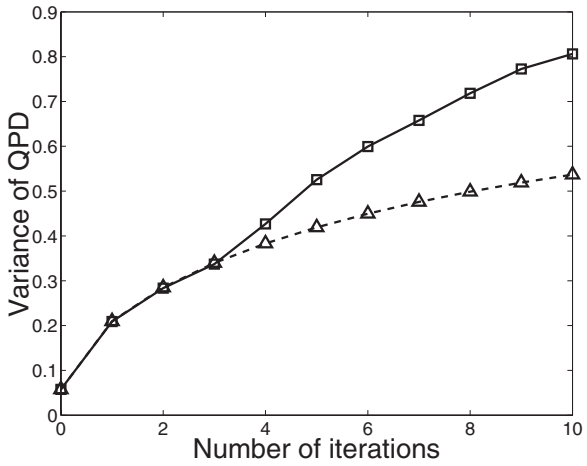

Fig. 4. Curves of the quadrature phase variance as a function of the number of interactions for the grid-length $\Delta\phi=0.2$ rad. The squares connected to the solid curve denotes the quantum walk, and the triangles connected to the dashed curve denotes the classic walk.

tical to that of the classic walk for the initial three iterations, and the initial values of both variances are nonzero owing to the width of the initial coherent state. However, beyond three iterations the quadratic speed up of phase diffusion for the quantum walk surpasses that for the classic walk. From Fig. 4 we also see that the spreading rate of the quantum walk is approximately linear from three to ten iterations. Note that the QPD gives a good approximation of the phase distribution only for small ϕ. For larger ϕ or beyond ten iterations the practical spreading rate will decrease.

The most important merit of the EIT-based system is the high transmission ratio for the probe field passing through the atomic cells. The reason for such high transmission is that the absorption of the probe field is greatly suppressed owing to the EIT-effect, and there are nearly no reflection losses at the entrance plane since the index of refraction of the atomic gas is close to unity. As is well known, wave plates can also produce phase shift, where the absorption effect is negligible owing to the frequency of the probe field that is far away from the resonant regime. However, there are serious reflection losses owing to a larger reflection index of the plates. Specifically, the ratio of the reflection losses is given by $[(n-1)/(n+1)]^2$; here we have assumed that the incident field is orthogonal to the entrance plane and n is the reflection index of the plates. If we take $n\simeq 1.54$ (quartz wave plates), the ratio of the reflection losses is 4.5% for each plate, i.e., the transmission ratio is 95.5%, which is lower than that of a single atomic cell reaching 99.5% ($T_+=T_-=0.995$). For realizing a QRW, it usually needs more wave plates than atomic cells, thus the apparatus using wave plates will be much less efficient. Another important merit of the EIT-based system is that the rotation angle for each single cell, i.e., the grid-length, can be easily controlled by adjusting parameters, such as the magnetic field and coupling field intensity. We can implement QRWs on various graphics (line or circle) without changing the system.

4. DISCUSSION AND SUMMARY

The motivation of this paper is to present a novel experimental scheme for QRW that is simple in principle and easy to realize practically. In our scheme the implementation of QRW is realized by using a Rubidium atomic gas with a double ladder EIT configuration, which is very different from all QRW schemes proposed until now. The EIT scheme has many important advantages in comparison with the previous schemes [11–18] for QRW. One of them is that the EIT system has a very high transmission rate for the probe field passing through atomic gas cells, which is very important for implementing a many-step QRW. The reason for such high transmission is that the absorption of the probe field is greatly suppressed by the EIT-effect induced by the control field, and there is nearly no reflection loss at the entrance plane. Another advantage of the EIT-based system is that such a system is simple and can be manipulated actively in a controllable way. We can implement QRWs on various graphics without changing the system.

In conclusion, in this paper we have proposed a scheme for implementing the QRW in a cold five-state atomic system via EIT. From the optical Bloch equations that describe the dynamics of electromagnetic field and atomic population and coherence, we have shown that two circular components of the probe field have different dispersion properties and hence acquire different phase-shift modifications when passing through the atomic cells. We have demonstrated that the quantum coherence and interference owing to the EIT effect lead to a very low absorption of the probe field and hence provide a possibility of implementing enough iterations and thus realizing a many-step phase-shift QRW. We have carried out a detailed investigation on how to implement the quantum walk based on realistic cold atomic systems. Our scheme may be used to experimentally highlight the difference between the quantum and classical walks and may have a promising application for quantum computation.

ACKNOWLEDGMENTS

The authors thank L. Deng for helpful discussions. This work was supported by the National Natural Science Foundation of China (NNSFC) under grants 10474055, 10588402, 10434060, and 10674060, the National Basic Research Program of China (973 Program) under grants 2005CB724508 and 2006CB921104, the Science and Technology Commission of Shanghai Municipality under grants 05PJ14038, 06JC14026, and 04DZ14009.

REFERENCES

1. M. A. Nielsen and I. L. Chuang, *Quantum Computation and Quantum Information* (Cambridge U. Press, 2000).
2. D. R. Simon, "On the power of quantum computation," SIAM J. Comput. **26**, 1474–1483 (1997).
3. P. W. Shor, "Polynomial-time algorithms for prime factorization and discrete logarithms on a quantum computer," SIAM J. Comput. **26**, 1484–1509 (1997).
4. L. K. Grover, "Quantum mechanics helps in searching for a needle in a haystack," Phys. Rev. Lett. **79**, 325–328 (1997).
5. Y. Aharonov, L. Davidovich, and N. Zagury, "Quantum random walks," Phys. Rev. A **48**, 1687–1690 (1993).
6. J. Kempe, "Quantum random walks: an introductory overview," Contemp. Phys. **44**, 307–327 (2003).
7. E. Farhi and S. Gutmann, "Quantum computation and decision trees," Phys. Rev. A **58**, 915–928 (1998).

8. A. M. Childs, E. Farhi, and S. Gutmann, "An example of the difference between quantum and classical random walks," Quantum Inf. Process. **1**, 35–43 (2002).
9. N. Shenvi, J. Kempe, and K. B. Whaley, "Quantum random-walk search algorithm," Phys. Rev. A **67**, 052307 (2003).
10. A. M. Childs and J. Goldstone, "Spatial search by quantum walk," Phys. Rev. A **70**, 022314 (2004).
11. B. C. Travaglione and G. J. Milburn, "Implementing the quantum random walk," Phys. Rev. A **65**, 032310 (2002).
12. B. C. Sanders, S. D. Bartlett, B. Tregenna, and P. L. Knight, "Quantum quincunx in cavity quantum electrodynamics," Phys. Rev. A **67**, 042305 (2003).
13. T. Di, M. Hillery, and M. S. Zubairy, "Cavity QED-based quantum walk," Phys. Rev. A **70**, 032304 (2004).
14. P. Zhang, X. Ren, X. Zou, B. Liu, Y. Huang, and G. Guo, "Demonstration of one-dimensional quantum random walks using orbital angular momentum of photons," Phys. Rev. A **75**, 052310 (2007).
15. P. K. Pathak and G. S. Agarwal, "Quantum random walk of two photons in separable and entangled states," Phys. Rev. A **75**, 032351 (2007).
16. P. L. Knight, E. Roldán, and J. E. Sipe, "Quantum walk on the line as an interference phenomenon," Phys. Rev. A **68**, 020301(R) (2003).
17. W. Dür, R. Raussendorf, V. M. Kendon, and H. J. Briegel, "Quantum walks in optical lattices," Phys. Rev. A **66**, 052319 (2002).
18. C. M. Chandrashekar, "Implementing the one-dimensional quantum (Hadamard) walk using a Bose–Einstein condensate," Phys. Rev. A **74**, 032307 (2006).
19. K. Eckert, J. Mompart, G. Birkl, and M. Lewenstein, "One- and two-dimensional quantum walks in arrays of optical traps," Phys. Rev. A **72**, 012327 (2005).
20. J. Du, H. Li, X. Xu, M. Shi, J. Wu, X. Zhou, and R. Han, "Experimental implementation of the quantum random-walk algorithm," Phys. Rev. A **67**, 042316 (2003).
21. C. A. Ryan, M. Laforest, J. C. Boileau, and R. Laflamme, "Experimental implementation of a discrete-time quantum random walk on an NMR quantum-information processor," Phys. Rev. A **72**, 062317 (2005).
22. S. E. Harris, "Electromagnetically induced transparency," Phys. Today **50**, 36–42 (1997).
23. M. Fleischhauer, A. Imamoglu, and J. P. Marangos, "Electromagnetically induced transparency: optics in coherent media," Rev. Mod. Phys. **77**, 633–673 (2005) (and references therein).
24. Y. Wu and L. Deng, "Ultraslow optical solitons in a cold four-state medium," Phys. Rev. Lett. **93**, 143904 (2004).
25. Y. Wu and L. Deng, "Ultraslow bright and dark optical solitons in a cold three-state medium," Opt. Lett. **29**, 2064–2066 (2004).
26. G. Huang, L. Deng, and M. G. Payne, "Dynamics of ultraslow optical solitons in a cold three-state atomic system," Phys. Rev. E **72**, 016617 (2005).
27. C. Hang, G. Huang, and L. Deng, "Generalized nonlinear Schrödinger equation and ultraslow optical solitons in a cold four-state atomic system," Phys. Rev. E **73**, 036607 (2006).
28. C. Hang and G. Huang, "Weak-light ultraslow vector solitons via electromagnetically induced transparency," Phys. Rev. A **77**, 033830 (2008).
29. C. Ottaviani, D. Vitali, M. Artoni, F. Cataliotti, and P. Tombesi, "Polarization qubit phase gate in driven atomic media," Phys. Rev. Lett. **90**, 197902 (2003).
30. S. Rebić, D. Vitali, C. Ottaviani, P. Tombesi, M. Artoni, F. Cataliotti, and R. Corbalán, "Polarization phase gate with a tripod atomic system," Phys. Rev. A **70**, 032317 (2004).
31. A. Joshi and M. Xiao, "Phase gate with a four-level inverted-Y system," Phys. Rev. A **72**, 062319 (2005).
32. C. Hang, Y. Li, L. Ma, and G. Huang, "Three-way entanglement and three-qubit phase qate based on a coherent six-level atomic system," Phys. Rev. A **74**, 012319 (2006).
33. I. Friedler, D. Petrosyan, M. Fleischhauer, and G. Kurizki, "Long-range interactions and entanglement of slow single-photon pulses," Phys. Rev. A **72**, 043803 (2005).
34. N. J. Cerf, C. Adami, and P. G. Kwiat, "Optical simulation of quantum logic," Phys. Rev. A **57**, R1477–R1480 (1998).